Process integration of Calcium-Looping thermochemical energy storage system in concentrating solar power plants

C. Ortiz [a, *], M.C. Romano [b], J.M. Valverde [a], M. Binotti [b], R. Chacartegui [c]

[a] Facultad de Física, Universidad de Sevilla, Avenida Reina Mercedes s/n, 41012, Sevilla, Spain
[b] Politecnico di Milano - Dipartimento di Energia, Via Lambruschini 4, 20156, Milano, Italy
[c] Escuela Técnica Superior de Ingeniería, Universidad de Sevilla, Camino de los Descubrimientos s/n, 41092, Sevilla, Spain

The Calcium-Looping process is a promising thermochemical energy storage method based on the multicycle calcination-carbonation of $CaCO_3$-CaO to be used in concentrated solar power plants. When solar energy is available, the $CaCO_3$ solids are calcined at high temperature to produce CaO and CO_2, which are stored for subsequent utilization. When power is needed, these reaction by-products are fed into a carbonator reactor where energy is released from the exothermic carbonation reaction. In com-parison with currently commercial energy storage systems, such as solar salts, the Calcium-Looping process presents several benefits such as the feasibility to work at significantly higher power cycle temperatures, a higher energy storage density and the possibility to store energy in the medium-long term. The present manuscript analyzes a number of novel Calcium-Looping configurations for energy storage combined with CO_2 cycles in a solar tower plant. The high overall efficiencies achieved (32–44%, defined as the ratio of net electric power production to net solar thermal power entering the calciner) indicate a potential interest for the integration of the Calcium-Looping process in Concentrating Solar Power Plants, although major technological challenges related to the design of the solar receiver and of the high temperature solids handling devices remain to be faced.

Keywords:
Calcium looping
CO_2 cycle
CSP
Energy storage

1. Introduction

Dispatchability is a main challenge for the commercial deployment of intrinsically variable major renewable energies such as wind and solar. Thus, efficient, cheap and non-toxic thermal energy storage (TES) is a key issue for Concentrating Solar Power (CSP) plants to provide a significant share of electricity generation. Currently, over 40% of commercial CSP plants around the world incorporate TES systems typically based on a two-tank TES system to use the sensible heat stored in molten salts, which allows CSP plants to operate up to 15 h in the absence of solar radiation [1].

In the last years, research on Thermochemical Energy Storage (TCES) systems as an alternative to molten salts has gained a considerable momentum [2]. TCES applied to CSP uses the heat available in the solar receiver to drive an endothermic reaction. When energy is needed, the by-products of the reaction are brought together at the necessary conditions for the reverse exothermic reaction to occur, which releases the previously stored chemical energy for power production. Main advantages of TCES over TES and PCMs are the possibility of storing energy in the long term [3] and the high energy density potentially achievable [4]. Many TCES systems are being analyzed as candidates for energy storage in CSP plants [5], among which we find systems based on hydroxides (e.g. $Ca(OH)_2$ [6]), metal redox (e.g. Co_3O_4 [7]), carbonates (e.g. $CaCO_3$ [8], $SrCO_3$ [9,10]), hydrides (e.g. MgH_2 [11]), ammonia [12], sulfur [13] or organic compounds (e.g. CH_4 [14]). A proper selection of the TCES system is crucial. In order to compare the different TCES systems, a general criterion was proposed by Wentworth and Chen [15].

Among the diverse thermochemical systems for energy storage, the cyclic calcination-carbonation of $CaCO_3$-CaO (Eq. (1)) stands as a promising method for CSP applications [16–20].

$$CaCO_{3(s)} \rightleftarrows CaO_{(s)} + CO_{2(g)} \quad \Delta H_r^0 = 178\ kJ/mol \tag{1}$$

The Calcium-Looping (CaL) process shows a number of important benefits for TCES in CSP such as: i) high turning temperature, which allows using high efficiency power cycles [21] thus

* Corresponding author.
E-*mail address:* cortiz7@us.es (C. Ortiz).

Published Journal Article available at: https://doi.org/10.1016/j.energy.2018.04.180

overcoming the limitations imposed by the degradation of molten salts at temperatures near ~600 °C, ii) high energy density [19], iii) the use of a well-known process and already mature technology originally developed for the cement and lime industry [22–24], iv) the low price, wide availability and non toxicity of natural limestone (near 100% $CaCO_3$) that may be employed as CaO precursor [25–27].

The CSP-CaL integrated process starts with the decomposition of $CaCO_3$ in a solar calcination reactor (calciner) where heat is supplied by concentrated solar radiation. In this regard, the CaL process is especially suited for CSP plants with tower technology where the attainable temperatures fit in the necessary range to achieve fast $CaCO_3$ decomposition (above 700 °C depending on the CO_2 partial pressure in the calciner environment [28]). The calcination by-products (CaO and CO_2) are sent to storage vessels and, when needed, circulated into a carbonator reactor wherein energy is recovered from the exothermic carbonation reaction.

The CSP-CaL integration, although already proposed as a concept in the late 1970s [29], has not been analyzed in detail until quite recently. Several solar calcination reactors have been proposed and tested [30–33]. Moreover, a number of studies have been reported regarding Ca-based materials behavior for TCES [20,34,35]. Edwards et al. [36] developed a CSP-CaL integration scheme in which the carbonator heat is transferred to a CO_2/air stream used as working fluid in a Joule-Brayton open cycle. Chacartegui et al. [8] have more recently proposed a higher efficiency (up to 45%) CSP-CaL scheme optimized by a pinch analysis [37] wherein the TCES system is coupled to a closed CO_2 power cycle [21]. Another possibility would be integrating a supercritical CO_2 cycle (s-CO_2) [38–40] in an indirect way, as was analyzed in a previous work [21]. Previous schemes [38,41] take advantage of the energy storage capacity of CaL process within a post-combustion CO_2 system. Other works [42,43] have presented diverse schemes in which CSP is used to aid calcination when the CaL process is employed for CO_2 capture in a coal fired power plant.

The present manuscript goes beyond previous analyses on the CSP-CaL integration by investigating the performance of new process schemes. Regarding to previous works, the novel schemes analyzed in the present work consider high temperature solids storage, which simplifies the heat integration process while maintaining a high-energy storage potential. In this regard, a new expression to estimate the energy density of a thermochemical system based on gas-solid reactions is proposed, which considers not just the reaction enthalpy but also the size of the vessels needed for solids storage and material properties such as the bulk porosity of the granular solids. A simpler heat integration allows to use novel integration schemes with a design similar to state-of-the-art equipment. Starting from a simplified base case each modified layout seeks to increase the overall plant efficiency at the expense of introducing an additional degree of complexity and therefore a higher investment cost.

The manuscript is structured as follows: first a CSP-CaL plant is generally described. Main concepts, possibilities and limitations of the cycle, as well as the assumptions made along the analisys are addressed. In section 3, four novel CSP-CaL integration schemes are analyzed from mass and energy balances. Afterwards, a sensitivity analisys is carried out in order to assess the impact of the different assumptions on cycle efficiency. Results show that overall plant efficiencies, defined as the ratio of net electrical production to net thermal input entering the calciner (and therefore without considering solar receiver efficiency) vary in a wide range of 32–44% depending on the system complexity and cycle parameters.

2. CSP-CaL plant

2.1. Overall description

Fig. 1 shows a flow diagram of the CSP-CaL integrated system. The process starts in the calciner, where solar energy is used to carry out the calcination reaction that releases gaseous CO_2 and solid CaO as products. In the present work it is assumed that calcination can be fully achieved in the calciner [17,22]. According to chemical equilibrium [28], a temperature around 900 °C is sufficiently high to drive calcination at atmospheric pressure in short residence times. Such temperature can be attained, for example, in a solar particle receiver [44,45]. Several solar calciner reactors have been already proposed in literature [30–32,46] and experimentally tested up to 50 kW scale [47].

CaO generated in the solar calciner is stored in a CaO storage vessel, while hot CO_2 is cooled down in a heat exchanger network consisting in a heat recovery steam generator for a bottoming steam cycle and in possible solids preheater. Cooled CO_2 is stored in a pressurized CO_2 vessel or used as working fluid in the power cycle.

On the carbonator side, preheated CO_2 reacts with CaO by exothermic carbonation, which produces $CaCO_3$. The CO_2 mass flow rate entering in the carbonator ($F_{CO2,crb,in}$) is well above the stoichiometric need and the excess CO_2 ($F_{CO2,crb,out}$) is used as fluid carrier to evacuate the heat released by carbonation. Hot CO_2 effluent from the carbonator is expanded in the main CO_2 turbine (M-TURB) driving the CO_2 compressors and producing electric power. Expanded CO_2 stream is cooled in a heat exchanger network, which consists of a CO_2 cycle regenerator and may include solids preheaters. The cooled CO_2 is mixed with the cooled CO_2 generated in the calciner or from the CO_2 storage vessel and then compressed up to the carbonator pressure.

One of the main drawbacks of the CaL process is the progressive loss of activity toward carbonation in short residence times of the regenerated CaO as the number of cycles increases depending on the carbonation/calcination conditions employed [48]. Thus, only a fraction *X* of the total flow of CaO entering the carbonator ($F_{R,crb,in}$) reacts to produce $CaCO_3$ ($F_{CaCO3,crb}$), while *1-X* remains as unreacted CaO ($F_{CaO,unr}$). The average CaO conversion X is thus a critical material property for the simulations. CaO conversion is highly dependent on the carbonation-calcination conditions as well as on the CaO precursor [49]. The CaL process applied to post-combustion CO_2 capture, which most of the CaL research focused on, involves carbonation under low CO_2 partial pressure whereas calcination is carried out under high CO_2 concentration at temperatures around 950 °C. These conditions lead to a severe drop of the CaO conver-sion with the number of cycles, reaching a residual value of just around X = 0.07–0.08 [50]. However, CaL conditions for TCES in CSP are not the same as those employed for CO_2 capture. In the proposed CaL-CSP integration scheme (Fig. 1) both carbonation and calcination are carried out under a pure CO_2 atmosphere. According to previous works, CaO residual conversion is about X = 0.2 for carbonation under 100%CO_2 atmosphere and calcination at 725 °C (under low CO_2 partial pressure) for $CaCO_3$ particles larger than 45 μm [18]. A similar value of the residual conversion for CaO derived limestone is reported by Obermeier et al. [17], who per-formed calcination at 800 °C in air atmosphere and carbonation at 600 °C under pure CO_2 atmosphere. In the present work, a baseline value of X = 0.15 is assumed for the process simulations at sta-tionary conditions, which means that about 85% by weight of the CaO entering into the carbonator exits it as unreacted CaO. Never-theless, a sensitivity analysis on the average conversion will be performed in Section 4 to assess the dependency of the plant per-formance on the CaO conversion.

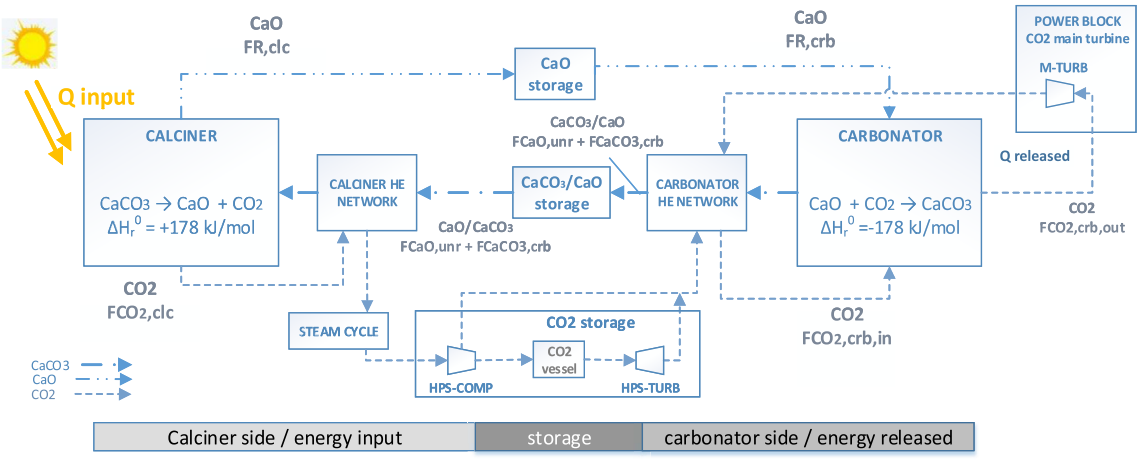

Fig. 1. CSP-CaL conceptual scheme.

Energy density values found in the literature for the CaL system vary widely. Some authors [4,38,51–53] report values around of 3–4 GJ/m^3 from the reaction enthalpy while other works [38,54,55] give values in the range of 0.9–2 GJ/m^3 by considering gas and solids vessels and/or that carbonation is not complete. Rhodes et al. [10] use an expression to calculate the energy density in each cycle as a function of the mass change observed in thermogravimetric experiments. However, it is interesting for practical purposes to address the size of the vessels needed for solids storage (i.e. taking into account the particles porosity and the packing density of solids), which is more closely connected with the capital costs of the energy storage system. To this end we propose Eq. (2), which can be applied to gas-solid TCES systems with the structure $AB_{(s)} \rightleftarrows A_{(s)} + B_{(g)}$ (for the CaL case: $AB = CaCO_3$; A = CaO; B=CO_2):

$$E_{den}\left[\frac{GJ}{m^3}\right] = \frac{X\cdot\left(\Delta H_R + \int_{T_{B,\ vessel}}^{T_{reactor}} c_{p,\ B}\,dT + \int_{T_{AB,\ vessel}}^{T_{A,\ vessel}} c_{p,AB}dT\right) + (1-X)\cdot\int_{T_{AB,\ vessel}}^{T_{A,\ vessel}} c_{p,A}dT}{\left(\frac{\nu_{AB}}{(1-\varepsilon_{AB})} + \frac{\nu_A}{(1-\varepsilon_A)}\right)\frac{1}{\varnothing} + X\cdot\nu_B} \tag{2}$$

where ΔH_R is the reaction enthalpy (GJ/kmol), $c_{p,\ i}$ is the specific heat of the component i (MJ/kmol·K), $T_{reactor}$ is the decomposition reaction temperature (K),$T_{i,\ vessel}$ is the storage temperature for of the component i (K), ν_i is the specific volume (m^3/kmol) of the component i at storage conditions, ε_i is the internal porosity of the component i and $\varnothing$ is the particle packing density, whose value is set to 0.6 as a typical value for the random loose packing fraction of irregularly shaped particles under gravity [56]. For the CaL specific case, it is assumed that particle size does not change by reversible reaction (which would affect mainly to its internal porosity) and therefore $\nu_{AB} = \nu_A$.

The CO_2 tank volume is a critical factor depending on the gas temperature and pressure. In the CSP-CaL integration scheme proposed elsewhere [8] CO_2 is stored at high pressure (75 bar) and atmospheric temperature (25 °C) to guarantee supercritical conditions and therefore minimize vessel size. The solids vessels capacity is highly influenced by the CaO conversion, since a high CaO reactivity reduces storage volume needs. Thus, the volumetric energy density of the entire CaL system is mainly dependent on the CO_2 storage conditions (pressure and temperature) and CaO conversion as shown in Fig. 2.

As shown in Fig. 2, considering supercritical conditions for CO_2 storage, the energy density of the entire system varies in a range of ~ 0.39–0.9 GJ/m^3 depending on CaO conversion. Fig. 2 also shows the energy storage density of a molten salt system by considering a two-tank configuration [57] and typical values of the temperature change (DT) in CSP plants [1]. As can be seen, the energy storage density of the entire CaL system is comparable to the molten salt technology for CaO conversions of 0.15, whereas it can be well above that of the molten salts system for higher CaO conversion.

2.2. Model assumptions

The main assumptions made to model the CSP-CaL plant are summarized in Table 1. All gas-gas heat exchangers are characterized by a minimum temperature difference (ΔT_{min}) of 15 °C, whereas gas-solids heat exchangers are assumed to achieve the same outlet temperature in both streams, assuming fluidized bed or entrained flow gas solid contactors. Auxiliaries power consumption in the carbonator and calciner sides are calculated as 0.8% of the heat rejected in coolers [58]. Solids transport is carried out by means of pneumatic conveying, which is an already mature technology to transport high temperature granular solids [59]. For Ca based particles and a typical transport length of 200 m, the estimated energy consumption is 20 MJ/ton [8]. Thermal loss in the storage system is highly dependent on the type of insulation employed. Thus, a thermal uncertainty parameter (including receiver and storage efficiencies) will be considered in the calculation of the solar to electric power efficiency.

In regard to the turbomachinery efficiencies, different values

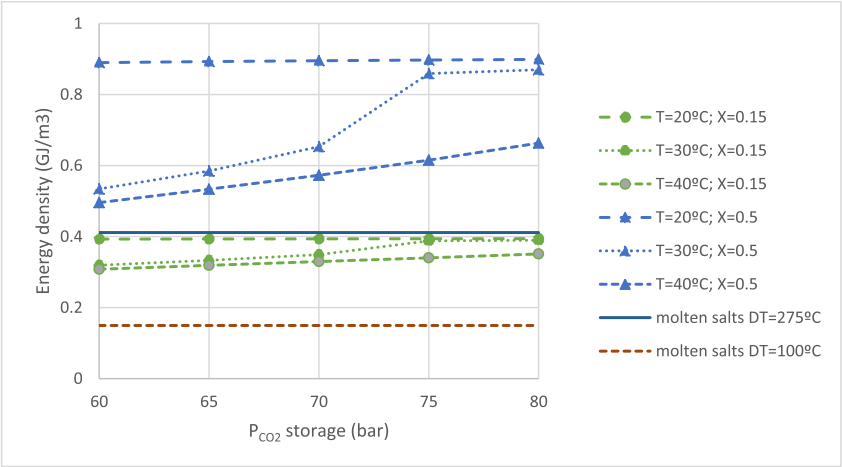

Fig. 2. Overall CaL energy storage density as a function of CO_2 storage conditions (pressure and temperature) and CaO conversion X. Solids storage temperature is assumed at 600 °C.

Table 1
Main assumptions in the CSP-CaL model.

Group	Parameter	Component	Value
Turbomachinery	Isentropic efficiency	Main CO_2 turbine (M-TURB)	0.9
		Main CO_2 compressor (M-COMP)	0.87
		High pressure storage turbine (HPS-TURB)	0.8
		High pressure storage compressor (HPS-COMP)	0.8
	Mechanical-electric efficiencies	Main CO_2 turbine (M-TURB)	0.98
		Main CO_2 compressor (M-COMP)	0.98
		CO_2 turbine (HPS-TURB)	0.96
		High pressure storage compressor (HPS-COMP)	0.96
	number of intercooling/reheating stages	High pressure storage compressor (HPS-COMP)	5
		Main CO_2 compressor (M-COMP)	0
		CO_2 turbine (HPS-TURB)	2
	Intercooling/reheating temperature	High pressure storage compressor (HPS-COMP)	40 °C
		High pressure storage turbine (HPS-TURB)	65 °C/100 °C
Heat exchangers	minimum temperature difference	gas-gas HX	15 °C
		CO_2-cooler	15 °C
	Pressure drops	coolers	1%
		HXG (both sides)	5%
		HRSG (hot side)	3%
		HRSG (cold side)	11%
		solid-gas HX (both sides)	3%
Reactors	Efficiency	Calciner	1
	Heat input	Calciner	100 MW
	Heat losses	Carbonator	1% of heat transferred
Storage vessels	Temperature losses	All	0 °C
	CO_2 storage conditions	CO_2 vessel	75 bar
			25 °C
Steam cycle	isentropic efficiency	Steam turbine (ST)	0.75
	Mechanical-electric efficiencies	Steam turbine (ST)	0.98
	condensing pressure	COND	0.075 bar
	evaporation pressure	HRSG	45 bar
	Super-heated steam temperature	HRSG	400 °C
Heat rejection	Auxiliaries electric power consumption	All coolers	0.8% of heat released

have been considered as a function of turbomachinery size and type (Table 1). Thus, higher isentropic and mechanical efficiencies are assumed for turbomachines with larger volume flow rate (M-TURB and M-COMP). The moderate heat input does not justify the adoption of complex configurations with high steam parameters for the heat recovery steam cycle. Thus, a simple superheated steam cycle with no reheat and moderate pressure and temperatures has been assumed.

Different operations in "sun" and "night" modes are simulated in this work. As previously stated, a Solar Multiple (SM) equal to 3 is assumed for the system design and for simplicity the day is considered composed by 8 h of sun, constantly providing 100 MWth to the calciner, and of 16 h of night. In the "sun" oper-ating mode the CO_2 mass flow entering the carbonator side ($F_{CO2,crb,in}$) is thus 1/3 the amount produced in the calciner ($F_{CO2,clc}$) whereas the remaining 2/3 are sent to a CO_2 storage vessel that is discharged during the "night" mode operations (2/3 of the day). In this simplified approach, the plant efficiency is therefore deter-mined as a weighted average of the performances in "sun" mode and "night" mode (Eq. (3)). A more detailed hour-by-hour calcu-lation with real solar radiation data and off-design plant analysis should be pursued for a rigorous yearly analysis.

$$\eta = \frac{\int_{24h} \dot{W}_{net}\, dt}{\int_{24h} \dot{Q}_{input}\, dt} = \frac{\dot{W}_{net,sun}\Delta t_{sun} + \dot{W}_{net,night}\,(24 - \Delta t_{sun})}{\dot{Q}_{input}\,\Delta t_{sun}} \quad (3)$$

In Eq. (4), $\dot{W}_{net}$ is the net electrical power produced by the system and $\dot{Q}_{input}$ is the solar power input in the calciner (100 MW for Δt_{sun} of 8 h). The electric power produced is computed for the "*sun mode*" ($\dot{W}_{net,sun}$) and the "*night mode*"($\dot{W}_{net,night}$), (Eqs. (4) and (5)):

$$\dot{W}_{net,sun} = \dot{W}_{M-TURB} + \dot{W}_{ST} - \dot{W}_{P} - \dot{W}_{M-COMP} - \dot{W}_{HPS-COMP} - \dot{W}_{PSOLCAL} - \dot{W}_{PSOLCAR} - \dot{W}_{AUXPOWCA} - \dot{W}_{AUXPOWCR} \quad (4)$$

$$\dot{W}_{net,night} = \dot{W}_{M-TURB} + \dot{W}_{HPS-TURB} - \dot{W}_{M-COMP} - \dot{W}_{PSOLCAR} - \dot{W}_{AUXPOWCR} \quad (5)$$

where $\dot{W}_{M-TURB}$ is the power produced by the main CO_2 turbine; $\dot{W}_{ST}$ and $\dot{W}_{P}$ are the power produced and consumed by the steam turbine and the pump of the steam cycle, respectively; $\dot{W}_{M-COMP}$ is the power consumed by the main CO_2 compressor; $\dot{W}_{HPS-COMP}$ is the power consumption by the high pressure intercooled CO_2 compressor for the storage system; $\dot{W}_{PSOLCAL}$ and $\dot{W}_{PSOLCAR}$ are the power consumptions due to solids transport in the calciner and carbonator sides, respectively; $\dot{W}_{AUXPOWCA}$ and $\dot{W}_{AUXPOWCR}$ are the auxiliary power consumptions in the calciner and carbonator sides, respectively; $\dot{W}_{HPS-TURB}$ is the power produced by the high pressure CO_2 turbine for expanding CO_2 from the storage to the carbonator pressure.

It is important to note that efficiency in our work strictly refers to the heat input to the calciner and therefore it does not take into account the thermal efficiency of the solar receiver, whose design and modelling is beyond the scope of this work.

3. CSP-CaL schemes

In order to analyze the most beneficial configuration as a tradeoff between efficiency and complexity 4 layouts have been analyzed. Case 1 is the base case, gas-solid heat exchangers are introduced in Case 2, an intercooled compression is added to Case 3 and, in Case 4, an ambient pressure carbonator is also employed. Calculations have been performed using the commercial software Aspen Plus™.

3.1. Base case

The proposed configuration for the base case is shown in Fig. 3. In the "sun" operation mode, solar energy is used in the calciner to bring the $CaCO_3$-rich solids stream up to reaction temperature (900 °C) for the calcination reaction to be achieved. The CO_2 pro-duced in the calcination (*g1* in Fig. 3) is sent to a heat recovery steam generator (HRSG) in order to use its sensible heat for power production by means of a simple superheated steam Rankine cycle. The cooled CO_2 stream (*g3*) is then compressed up to 3 bar in the main CO_2 compressor (M-COMP) and is split in two streams. A fraction of the CO_2 (1/3 of total) is sent directly to the carbonator (*g7a*), whereas the rest (*g4*) is further compressed up to 75 bar (HPS-COMP) and stored (CO_2 storage) for its use during the "night" operation mode. The CaO produced in the calciner (*c1*) is directly stored in the high temperature CaO storage vessel. Solids are stored at ambient pressure and therefore lock hoppers are needed for decoupling the pressure of the atmospheric solar receiver and of the storage vessel from the pressurized carbonator.

On the carbonator side, electric power is produced by means of a CO_2 closed Brayton cycle wherein a heat exchanger *HXG* is used as recuperator. For this base case, CO_2 is expanded from carbonator pressure to atmospheric pressure in the turbine with a pressure ratio of 3 ($PR = P_{carbonator}/P_{out,\ MTURB}$). The CO_2 mass flow rate entering the carbonator (*g9*) is well above the stoichiometric need for CaO carbonation and is controlled to achieve the target turbine inlet temperature. Thus, the CO_2 flow rate that does not react (*g10*) takes the heat released by the carbonation reaction. Carbonation has been modelled in the base case by considering a residual value of CaO conversion X = 0.15. Then, with the aim of analyzing the effect of CaO conversion on the plant performance a sensitivity analysis has been carried out. After the recuperator, the CO_2 stream is cooled by heat rejection to ambient and then compressed again in the low-pressure compressor (M-COMP) to close the Brayton power cycle.

As can be seen in Fig. 3, only gas-gas heat exchangers (HRSG, HXG) and coolers are considered in this base case, which simplifies the plant as compared to previously proposed CSP-CaL integrations [8], which made use of counter-flow gas-solid and solid-solid heat exchangers. This new configuration is therefore advantageous from the point of view of plant engineering, construction and operation. Main stream data for the base case is given in Appendix.

The energy balance resulting from the simulation of the base case is summarized in Table 2. This configuration shows an overall plant efficiency of 32.1%. As a consequence of the design criteria to keep a constant power production by the main turbine (M-TURB), a higher net power output is obtained in the "night mode" compared to the "sun mode". This is because the power consumed by the high-pressure CO_2 storage compressor (HPS-COMP) and by the auxiliaries for solids transport is not fully compensated by the power generated by the steam turbine. On the other hand, part of the CO_2 compression power is recovered in the "night mode" by the high-pressure CO_2 storage turbine (HPS-TURB). As a result, net power output in the "night mode" operation is 44% higher than in "sun mode" operation.

The third column in Table 2 (*"sun mode w/o storage"*) shows the energy balance of the plant when operated without storage. This case can be representative of i) the same plant designed with SM = 3 when operating with a solar radiation absorbed by the calciner equal to 1/3 of the design heat input or of ii) a plant designed with the same gross turbine power (M-TURB), SM = 1 and no TES. In this case, heat input to the calciner is 1/3 of the design power and the flow rate of CO_2 produced in the calciner matches the flow rate sent to the CO_2 cycle to compensate the CO_2 captured in the carbonator. In this operating mode, the power related to the turbomachines linked to the storage system (HPS-COMP and HPS-TURB) is zero. The overall plant efficiency obtained for this case is 33.9%. Thus, the efficiency penalty associated to the storage system sized with a solar multiple of 3 is 1.8% points.

As shown in Table 2, main heat rejections to ambient occur in the CO_2 cycle precooler (COOLER-3 in Fig. 3) and in the steam condenser (COND). In the case of COOLER-3, the CO_2 stream exiting the recuperator HXG (g12) is cooled from 154 °C down to 40 °C and part of this heat is used to heat up the CO_2 coming from the storage (HEATER). A non-negligible thermal power is also rejected to ambient by the high-pressure CO_2 cooler (COOLER-2), which is used to cool the compressed CO_2 (g5 stream) from the HP compressor (HPS-COMP) to a storage temperature of 25 °C and by the HPS-COMP intercoolers.

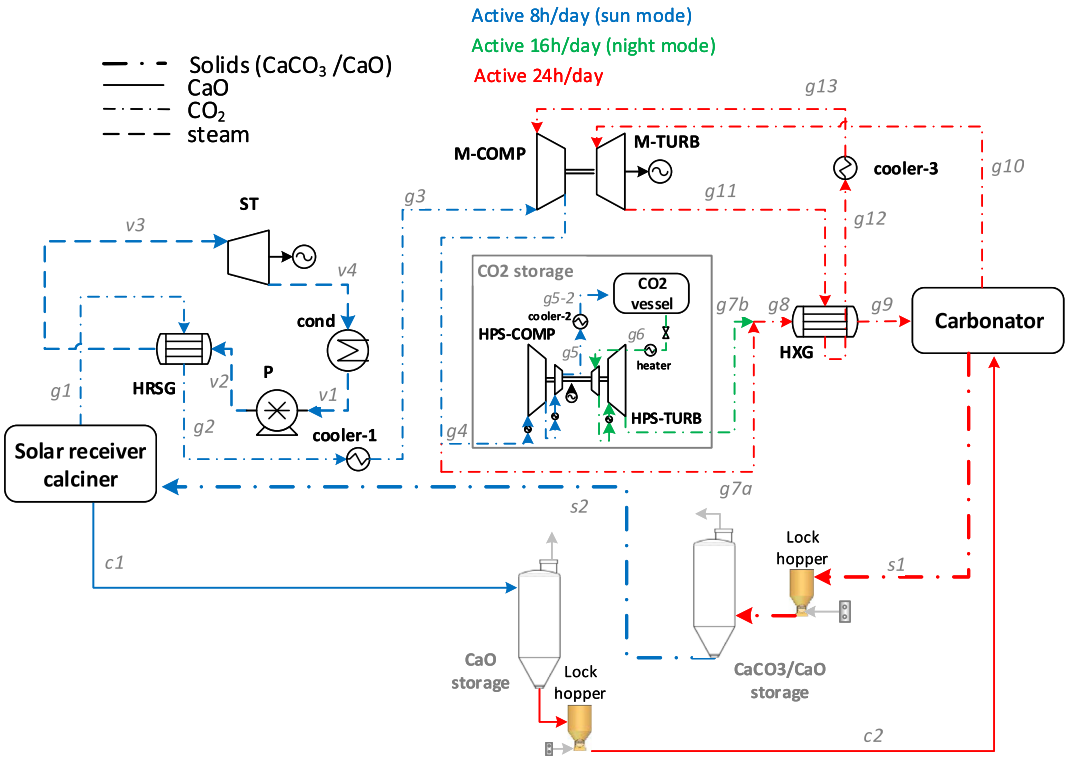

Fig. 3. Proposed configuration in this work for the CSP-CaL base case.

Table 2
Energy balance resulting from the simulations of the base case.

	Parameter	Base case (Fig. 3)		
		"sun mode"	"night mode"	"sun mode w/o storage"
	Solar thermal power to the calciner (MW_{th})	100	0	33.33
Heat exchangers Thermal Power(MWth)	HRSG	21.73	–	7.24
	COOLER-1	0.24	–	0.08
	COND	15.85	–	5.28
	HP-COMP (intercooler)	4.66	–	–
	COOLER-2	4.15	–	–
	HEATER	–	2.14	–
	TURB1 (interheater)	–	0.77	–
	COOLER-3	13.24	13.24	13.24
	HXG	75.91	75.91	75.91
Power production (MWe)	CO_2 storage turbine (HPS-TURB)	–	1.05	–
	Main CO_2 turbine (M-TURB)	23.92	23.92	23.92
	Steam Turbine (ST)	5.80	–	1.93
Power consumptions(MWe)	Steam cycle pump (P)	−0.04	–	−0.01
	Main CO_2 compressor (M-COMP)	−12.94	−12.22	−12.94
	CO_2 storage compressor (HPS-COMP)	−5.33	–	–
	Auxiliaries for heat rejection (calciner side)	−0.20	–	−0.04
	Auxiliaries for heat rejection (carbonator side)	−0.11	−0.11	−0.11
	Auxiliaries for solids transport calciner	−2.17	–	−0.72
	Auxiliaries for solids transport carbonator	−0.72	−0.72	−0.72
Net power (MWe)	$\dot{W}_{net,sun}$	**8.27**	**-**	**11.31**
	$\dot{W}_{net,night}$	**-**	**11.93**	**0**
Overall plant efficiency	η	**0.321**		**0.339**

3.2. *Case 2: addition of solid-gas heat exchangers*

Compared to the base case, case 2 (Fig. 4) incorporates the use of solid-gas heat exchangers on both calciner and carbonator sides. In this way, it is possible to make a more profitable use of the high temperature heat stored in the streams exiting the reactors, which leads to an improved thermal integration. Solids heating could be performed in a suspension preheater where gas and solids are sequentially contacted in risers and separated by cyclones, as usually performed in raw meal preheaters of cement plants [60]. All solid-gas heat exchangers have been modelled by assuming a co-flow arrangement and a same exit temperature of the gas and solids streams (as shown in Fig. 5).

GS-HE1 is used to exchange heat between the CO_2 stream exiting the calciner at 900 °C and the solids stream entering it, which must be brought to the calcination temperature, while heat

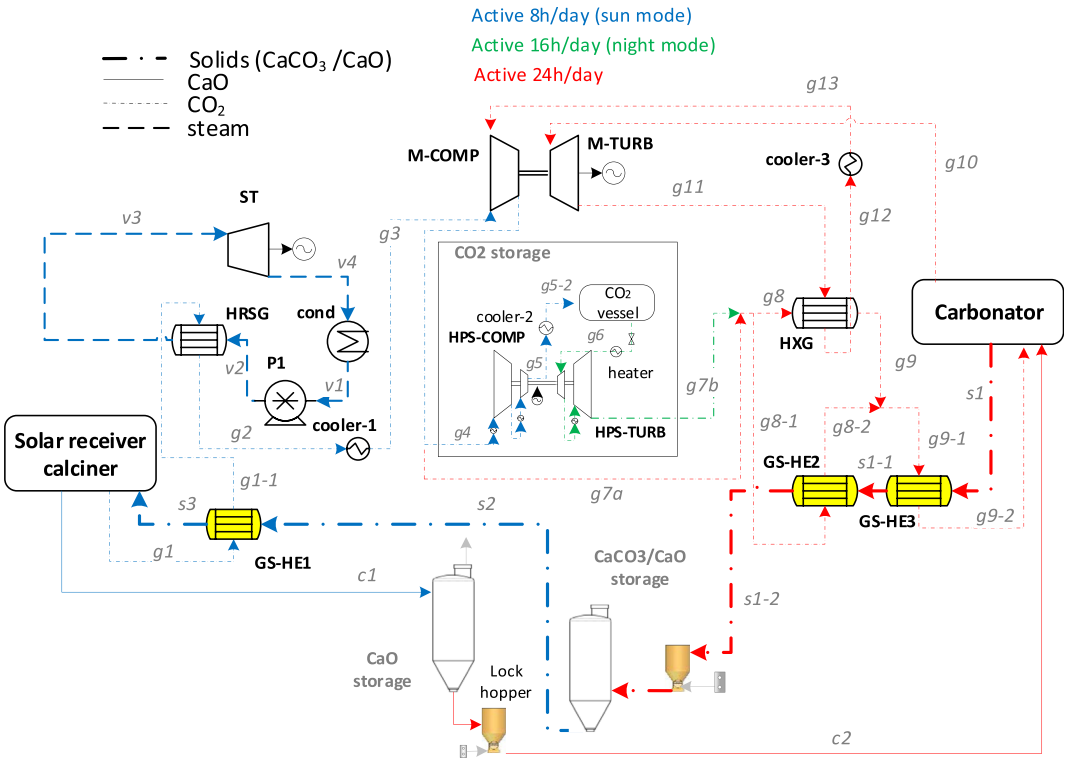

Fig. 4. CSP-CaL modified integration scheme (case 2).

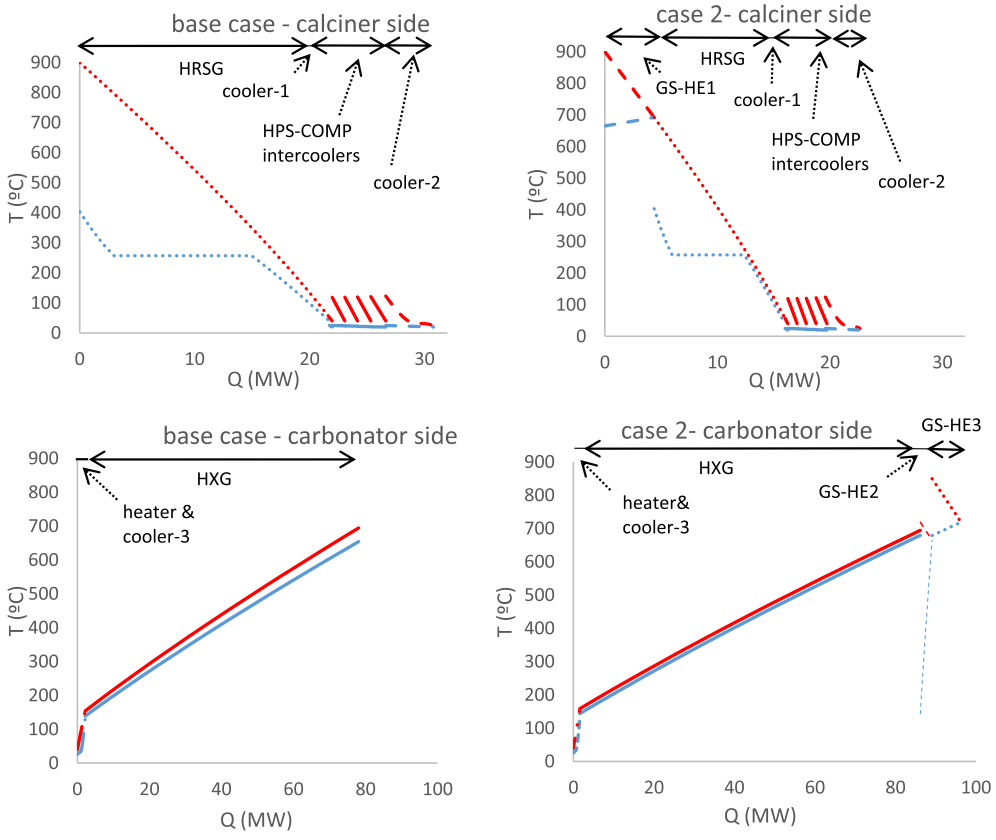

Fig. 5. TQ diagrams for calciner/carbonator sides in both the base case and case 2 configurations.

Table 3
Energy balance for the cases 2,3 and 4.

Parameter		Case 2			Case 3			Case 4		
		Including: solids heat exchangers			Including: solids heat exchangers Intercooled compression			Including: solids heat exchangers Intercooled compression P=Patm carbonation		
		"sun mode"	"night mode"	"sun mode w/o storage"	"sun mode"	"night mode"	"sun mode w/o storage"	"sun mode"	"night mode"	"sun mode w/o storage"
Solar thermal power (MW_{th})		100	0	33.33	100	0	33.33	100	0	33.33
Heat exchangers thermal Power (MWth)	HRSG	11.63	–	3.88	11.37	–	3.80	11.51	–	3.84
	GS-HE1	4.39	–	1.46	4.45	–	1.48	4.42	–	1.47
	COOLER-1	0.25	–	0.08	0.32	–	0.11	0.28	–	0.09
	COND	8.49	–	2.830	8.23	–	2.78	8.40	–	2.80
	HP-COMP (intercooler)	3.47	–	–	3.45	–	–	3.46	–	–
	COOLER-2	3.08	–	–	3.06	–	–	3.07	–	–
	HEATER	–	1.58	–	–	1.57	–	–	1.58	–
	TURB1 (interheater)	–	0.57	–	–	0.56	–	–	0.74	–
	COOLER-3	15.54	15.54	15.54	6.02	6.02	6.02	6.04	6.04	6.04
	HXG	84.60	84.60	84.60	93.27	93.27	93.27	93.68	93.68	93.68
	GS-HE2	2.91	2.91	2.91	3.17	3.17	3.17	3.04	3.04	3.04
	GS-HE3	7.19	7.19	7.19	7.15	7.15	7.15	7.17	7.17	7.17
Power inlet (MWe)	CO_2 storage turbine (HPS-TURB)	–	0.77	–	–	0.76	–	–	1.01	–
	Main CO_2 turbine (M-TURB)	26.87	26.87	26.87	26.64	26.64	26.64	26.77	26.77	26.77
	Steam Turbine (ST)	3.10	–	1.03	3.03	–	1.01	3.07	–	1.02
Power outlet (MWe)	Steam cycle pump (P)	−0.02	–	−0.01	−0.02	–	−0.01	−0.02	–	−0.01
	Main CO_2 compressor (M-COMP)	−14.67	−14.11	−14.67	−13.26	−12.75	−13.26	−13.28	−13.20	−13.28
	CO_2 storage compressor (HPS-COMP)	−3.98	–	0.00	−3.95	–	0.00	−3.96	–	0.00
	Auxiliaries heat calciner	−0.12	–	−0.02	−0.12	–	−0.02	−0.12	–	−0.02
	Auxiliaries heat carbonator	−0.12	−0.12	−0.12	−0.12	−0.12	−0.12	−0.12	−0.12	−0.12
	Auxiliaries solids transport calciner	−1.60	–	−0.53	−1.59	–	−0.53	−1.60	–	−0.53
	Auxiliaries solids transport carbonator	−0.53	−0.53	−0.53	−0.53	−0.53	−0.53	−0.53	−0.53	−0.53
Wnet	$\dot{W}_{net,sun}$	**8.94**	–	**12.01**	**10.09**	–	**13.18**	**10.21**	–	**13.30**
	$\dot{W}_{net,night}$	–	**12.88**	–	–	**14.01**	–	–	**13.92**	**-**
Overall plant efficiency	η		**0.347**	**0.360**		**0.381**	**0.395**		**0.381**	**0.399**

exchangers GS-HE2 and GS-HE3 are used to preheat the CO_2 stream entering the carbonator. As a consequence, solids are stored in the vessels at lower temperature and lock hoppers also operate at lower temperatures. Streams properties is reported in Appendix while the energy balance for this case is shown in Table 3.

Because of the preheating of the gas in GS-HE2 and GS-HE3, this enter the carbonator at higher temperature compared to the base case (719 °C instead 654 °C) and a higher CO_2 flow rate can pass across this reactor to carry the heat released by the carbonation reaction. As a result, the power produced by the main CO_2 turbine increases by a 12%. Fig. 5 shows the temperature-heat (TQ) diagrams for both the base case and case 2.

As shown in Fig. 5, a better heat integration is achieved in the calciner side for the case 2. An enhanced utilization of high-temperature stream temperature is achieved, with the conse-quent reduction in exergy loses. The lower storage temperature in the $CaCO_3$/CaO storage vessel also causes a reduction of the solids temperature at the inlet of the calciner (stream s3). Therefore, in the "sun mode", a higher portion of the heat provided to the calciner is taken as sensible heat of the solids stream and less power is available for the calcination reaction, which lowers the production of CaO and CO_2. The reduced flow rate of CO_2 combined with the lower temperature at the HRSG inlet (stream g1-1) after the solids preheater GS-HE1 causes a reduction of the steam generated and of the steam turbine power (−47% compared to the base case). The reduction of the solids flow rate and of the CO_2 flow rate generated in the calciner also lead to a reduction of consumption of the HP CO_2 storage compressor and the auxiliaries for calciner solids transport (−26%).

Regarding the energy balance, an overall plant efficiency of 34.7% has been obtained, i.e. 2.6% points higher than the base case efficiency. The calculated net efficiency without energy storage also increases to 36.0%. Due to the reduced consumption for CO_2 storage compression, the differences between these two calculated efficiencies and between the net power produced in "sun" and "night" modes are also reduced.

3.3. Case 3: introduction of solid-gas heat exchangers and intercooled compression

Compared with case 2, case 3 contemplates the use of an intercooled main CO_2 compressor, which allows reducing the consumption for CO_2 compression and achieving a higher cycle efficiency thanks to the presence of the regenerator. The low-pressure intercooled compressor is used to compress around 140 kg/s of CO_2 from atmospheric pressure to the carbonator pressure. In this case, two intercoolers are assumed with an inter-cooled temperature of 40 °C, leading to compressor outlet tem-peratures of 73 °C from each stage. This leads to a reduction of the CO_2 stream temperature at compressor outlet (*g8*) compared to case 2 (73 °C instead 143 °C), which allows for a higher heat ex-change in HXG and therefore a reduced need for cooling in cooler-3. Results for this configuration can be seen in Table 3. By using a 2 intercooled-stages main compressor (M-comp), electric

consumption is reduced by 6.8% and 8.8% in the "sun" and "night" modes, respectively, which implies an overall plant efficiency increase of 3.4%.

3.4. Case 4: carbonator at ambient pressure

Case 4 allows operating the carbonator at ambient pressure. As a benefit, high temperature lock hoppers for solids pressurization would not be necessary. On the other hand, hermetic machines and heat exchangers to avoid air in-leakages as well as larger turbomachines (to handle the higher volume flow rate), larger carbonator and larger heat exchangers (to compensate the decrease of heat transfer coefficient with gas density) must be employed. Moreover, it is expected to achieve a lower reaction rate in the carbonator, which is favored by high CO_2 pressure [61].

Fig. 6 shows the case 4 scheme. M-comp compresses the CO_2 stream coming from the carbonator (*g13*) up to atmospheric pressure (plus about 0.1 bar to overcome pressure drops). Unlike in previous layouts in which *g3* and *g13* compressions were made completely in the M-compressor, in case 4 the CO_2 coming from the calciner (*g3*) is simply blown by a fan and is directly sent to the carbonator side, without passing through the M-comp.

As shown in Table 3, there are no big differences in terms of efficiency between cases 3 and 4. Therefore, the most advantageous configuration between pressurized and atmospheric pressure carbonator must be chosen based on techno-economic considerations depending on the technical challenge and cost of a high temperature lock hopper system or the sealed components for a specific facility. The techno-economic analysis is being carried out by considering a quasi-stationary simulation to better assess the equipment sizes and costs and will be reported in a future publication. Note that all configurations have been modelled with $PR = 3$.

A higher temperature is achieved at the carbonator inlet in all cases where solid-gas heat exchangers are integrated (as shown in Appendix), which leads to a higher temperature of heat introduced in the thermodynamic cycle and therefore to a higher cycle efficiency. As a consequence, a larger mass flow rate of CO_2 can be heated up to 850 °C for power production. Thus, 133.5 kg/s of CO_2 enter in the main turbine for the base case whereas in case 4 this value is increased up to 151 kg/s.

Compared to the base case (where the global efficiency is 32.1%), the overall plant efficiency increases for all the modified configurations. As mentioned in the base case, also in these schemes an efficiency increase is achieved when no storage and SM = 1 are considered as the high-pressure compressor is not used. Thus, it is important to point out that the base operation mode selected for the simulations ("*sun mode*", SM = 3) represents the worst scenario since throughout the day the solar power hitting the solar receiver will vary and therefore most of the time less than 100 MW_{th} will be produced in the solar field. In practical operation conditions, the net global efficiency achieved in each case will be comprised between the weighed efficiency (1/3–2/3) and the efficiency in "*sun mode w/o storage*" depending on the characteristics of solar radiation for the selected site and on the solar field off-design performance.

4. Sensitivity analysis and discussion

This section is devoted to compare the performance of the four configurations proposed for different gas cycle pressure ratio and

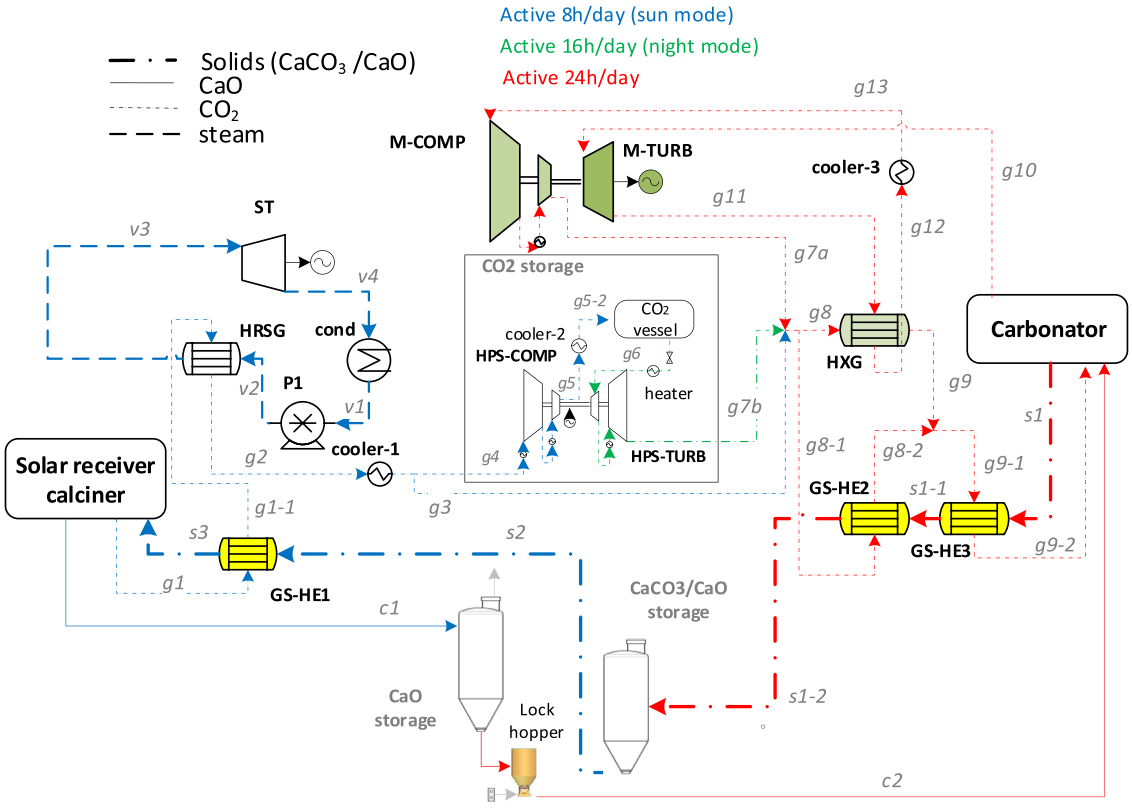

Fig. 6. CSP-CaL modified integration scheme (case 4).

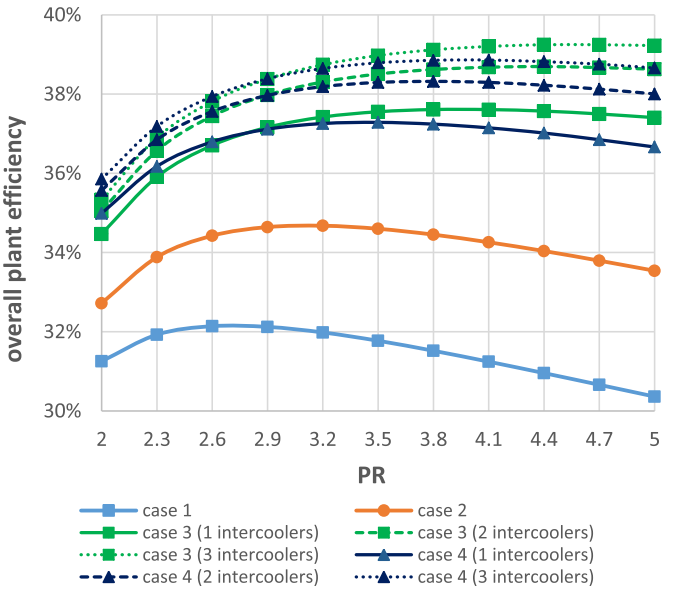

Fig. 7. Sensitivity analysis on pressure ratio (PR).

number of main compressor intercoolers from the overall efficiency perspective. Moreover, to further explore the CSP-CaL integration, a sensitivity analysis has been carried out on case 3 about the effect of the turbine inlet temperature, CaO conversion, steam cycle condi-tions, turbomachinery efficiency, minimum ΔT in the main CO_2 heat exchanger, and CaO-CO_2 storage conditions.

4.1. Effect of pressure ratio

In this section, all previous schemes are compared to analyze the most advantageous configuration. To this end, the pressure ratio (*PR*), defined as the ratio of the carbonator pressure to the turbine outlet pressure, has been chosen as dependent variable. Note that in the previous section all configurations are analyzed at $PR = 3$.

Fig. 7 shows the resulting overall plant efficiency as a function of the pressure ratio for the different cases and assuming a different number of intercooling stages in the main CO_2 compressor (for cases 3 and 4 only). As can be seen, cases 3 and 4 clearly show a higher efficiency than cases 1 and 2, particularly for higher pressure ratios. This illustrates the benefits of using the multi-stage inter-cooled compression combined with the gas cycle regenerator HXG.

The simplest configuration (base case) reaches the maximum efficiency with PR of about 2.8, whereas in case 2 (where gas-solids heat exchangers are considered) efficiency is enhanced to near 35% at PR = 3.2. Gas-solids preheating allows increasing the temperature of solids stream entering the carbonator and a higher CO_2 flow rate can be expanded in the main turbine (M-TURB). Thanks to the inter-cooled compression, the overall efficiency is further increased in case 3, reaching a value near 40% at PR between 4 and 5. Compared to previously reported CSP-CaL schemes [8,21], this relatively high efficiency is achieved in case 3 with a configuration of lower technical complexity and based on equipment already used in the cement industry, which would imply also a lower system cost.

4.2. Effect of turbine inlet temperature (TIT), CaO average conversion (X) and pressure ratio

As it was shown in Fig. 7, there is a carbonator pressure for which the integration efficiency reaches a maximum, which justifies the relevance of an analysis on the pressure and temperature conditions in the carbonator to determine the optimal CaL-power cycle integration.

Since the carbonator is directly connected to the turbine inlet, increasing the carbonator temperature leads to a higher power cycle efficiency. However, the maximum temperature in the carbonator is limited by the thermodynamic equilibrium of the calcination-carbonation reaction (Eq. (1)). According to thermochemical data, the equilibrium temperature T_{eq} is related to the CO_2 partial pressure in the carbonator environment P by means of Eq. (6) [28]:

$$T_{eq} = -\frac{20474}{\ln\left(\frac{P}{4.137\cdot 10^7}\right)} \tag{6}$$

where P is measured in bar and T_{eq} in K. Thus, for a given value of P there is a maximum carbonator temperature (T_{max}=T_{eq}) above which the CO_2 partial pressure is not sufficiently high for the reaction to be shifted toward carbonation (Fig. 8). Since in all considered cases carbonation is carried out under a pure CO_2 atmosphere, CO_2 partial pressure coincides with the carbonator absolute pressure.

In order to get a grip on the role of turbine inlet temperature and pressure ratio, case 3 was simulated by considering the cycle without storage, thus all the CO_2 and CaO exiting the calciner side is sent to power production (SM = 1). The analysis also contemplates several values of the average CaO conversion (X). This analysis is important because of the high uncertainty on the CO_2 carrying capacity of CaO under the carbonation and calcination conditions assumed in this work. Moreover, as discussed in section 2, CaO conversion is highly dependent on the carbonator-calciner conditions as well as on the CaO precursor.

Table 4 shows the energy balance obtained by varying the carbonator temperature (and therefore the TIT) and the CaO average conversion. Note that for a better understanding, these balances are referred to the conditions without storage and therefore consumption of CO_2 storage compressor and power generated by the CO_2 storage turbine are zero.

As expected, an increase in either CaO conversion or TIT leads to a higher overall plant efficiency. If TIT is raised from 850 °C to 950 °C the overall efficiency is enhanced by about 1.2% and 2.7%points for X = 0.1 and X = 0.4, respectively. As shown in Table 4,

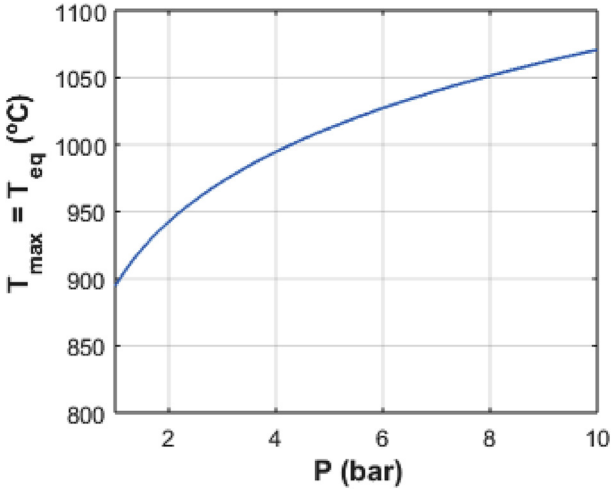

Fig. 8. Maximum carbonator temperature as a function of CO_2 partial pressure in the carbonator atmosphere according to thermodynamic equilibrium (Eq. (6)).

Table 4
Energy balance for the case 3 as a function of TIT and X (SM = 1, PR = 3.5).

	Parameter	X = 0.1		X = 0.4	
		TIT = 850 °C	TIT = 950 °C	TIT = 850 °C	TIT = 950 °C
	Solar thermal power (MW_{th})	33.33	33.33	33.33	33.33
Heat exchangers (MWth)	HRSG	3.368	4.796	4.138	4.859
	GS-HE1	1.279	0.868	2.072	1.693
	COOLER-1	−0.097	−0.111	−0.128	−0.137
	COND	−2.457	−3.499	−3.019	−3.545
	COOLER-3	−5.943	−5.157	−5.719	−5.104
	HXG	80.923	83.050	78.760	82.764
	GS-HE2	2.891	4.299	3.261	4.077
	GS-HE3	9.108	10.804	4.975	5.601
Power inlet (MWe)	Main CO_2 turbine (M-TURB)	27.226	26.044	26.479	25.943
	Steam Turbine (ST)	0.899	1.280	1.105	1.297
Power outlet (MWe)	Steam cycle pump (P)	−0.006	−0.009	−0.008	−0.009
	Main CO_2 compressor (M-COMP)	−13.523	−12.030	−13.335	−12.083
	Auxiliaries heat calciner	−0.020	−0.029	−0.025	−0.029
	Auxiliaries heat carbonator	−0.120	−0.105	−0.117	−0.105
	Auxiliaries solids transport calciner	−0.677	−0.824	−0.275	−0.291
	Auxiliaries solids transport carbonator	−0.677	−0.824	−0.275	−0.291
Carbonator heat (MWth)	carbonation heat	19.253	23.442	25.717	27.137
	reactants preheating (sensible heat)	2.217	−4.698	−0.320	−2.573
	losses	−0.194	−0.234	−0.252	−0.274
	carbonator heat to power cycle	21.276	18.510	25.145	24.290
Power output CO_2 cycle (MWe)		13.704	14.014	13.144	13.860
Power output steam cycle (MWe)		0.893	1.271	1.097	1.288
Overall plant efficiency (η)		**0.393**	**0.405**	**0.406**	**0.433**

Table 5
Trends in selected streams by varying X and TIT.

X	TIT = 850 °C				TIT = 950 °C			
	g10 (kg/s)	g1 (kg/s)	s2 (T°C)	s3 (T°C)	g10 (kg/s)	g1 (kg/s)	s2 (T°C)	s3 (T°C)
0.1	127.43	4.93	673.17	692.25	111.75	6.00	769.82	780.31
0.15	126.18	5.49	647.71	676.88	111.73	6.28	736.96	755.71
0.2	125.39	5.86	627.67	666.43	111.59	6.48	712.35	738.90
0.25	124.87	6.11	611.42	659.11	111.51	6.64	692.97	726.95
0.3	124.48	6.31	597.72	653.70	111.42	6.76	676.86	717.88
0.35	124.19	6.46	586.25	649.83	111.37	6.86	663.22	710.84
0.4	123.95	6.58	576.19	646.81	111.32	6.94	651.52	705.28

power consumptions due to solids conveying are the same in the calciner and carbonator sides since storage is not considered in this analysis.

As can be seen, the steam cycle production is enhanced with the carbonator temperature. As the carbonator temperature is raised, the temperature of the solids entering the calciner (s2) increases as well, reducing the sensible heat required to heat them up to 900 °C or, equivalently, increasing the $CaCO_3$ flow rate to achieve full calcination. Thus, a higher amount of CO_2 can be produced in the calciner (see *g1* stream in Table 5). Furthermore, the net power produced by the CO_2 closed cycle is also enhanced with the carbonator temperature. An increase in CaO conversion enhances the steam cycle production albeit it does not lead to a higher net power output in the CO_2 closed cycle. This is mainly due to the reduction of CO_2 temperature at the carbonator inlet (Table 5) because of the lower solids to gas ratio in the CO_2 preheaters, which leads to a lower temperature of heat introduction into the gas cycle and therefore to a decrease of the cycle efficiency. A reduction of the CO_2 temperature at the carbonator inlet causes that a higher amount of carbonation heat is used to bring the reactants to the carbonation temperature and therefore, a lower amount of CO_2 can be recirculated (*g10)*. Table 4 shows the carbonator heat used to preheat the reactants to the carbonator temperature. By considering TIT = 850 °C and X = 0.1, a high amount of solids (compared with the X = 0.4 case) is circulated from the calciner (at 900 °C) to the carbonator, whose temperature is reduced. Therefore, this solids stream carries additional heat from the calciner to be used in the power cycle (as can be seen by the positive sign of the reactants pre-heating thermal power in Table 4).

Fig. 9 shows the global CSP-CaL efficiency as a function of X and TIT.

The different trends followed by the overall efficiency with X in the cases of TIT = 850 °C and 950 °C may be explained by an analysis of the CaO temperature entering the carbonator from the calciner at 900 °C. In the case of TIT = 950 °C, a part of the energy released in the carbonator must be used to bring the solids up to the carbonator temperature, being this effect more important when X is reduced (see reactants preheating power in Table 4). In the case of TIT = 850 °C, it is not necessary to heat up the solids since these come from the calciner at higher temperature, and therefore the loss of efficiency by reducing the CaO conversion is mitigated. Fig. 9 shows also efficiency results obtained by including or not auxil-iaries' consumption. In regard to increasing the CaO conversion, the energy consumption linked to solids conveying is decreased, which

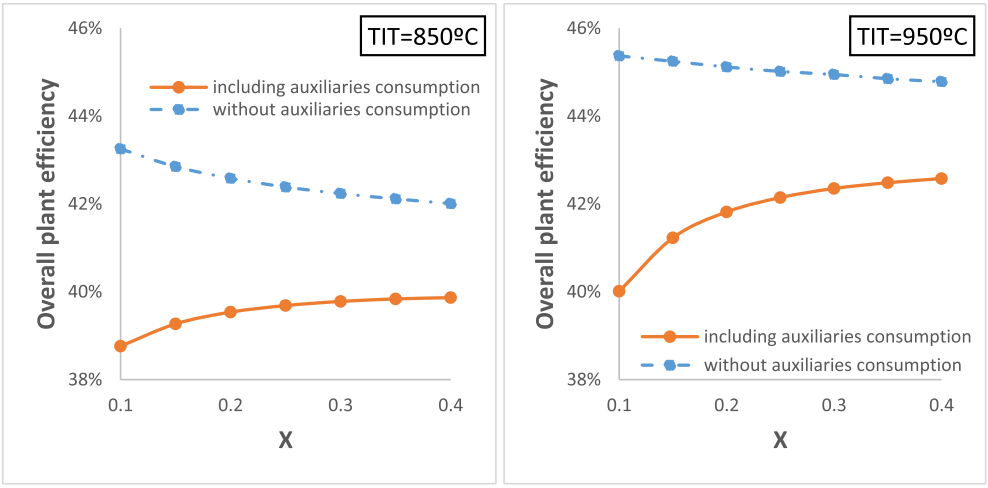

Fig. 9. Overall plant efficiency as a function of X for two different TIT (no storage is considered: SM = 1).

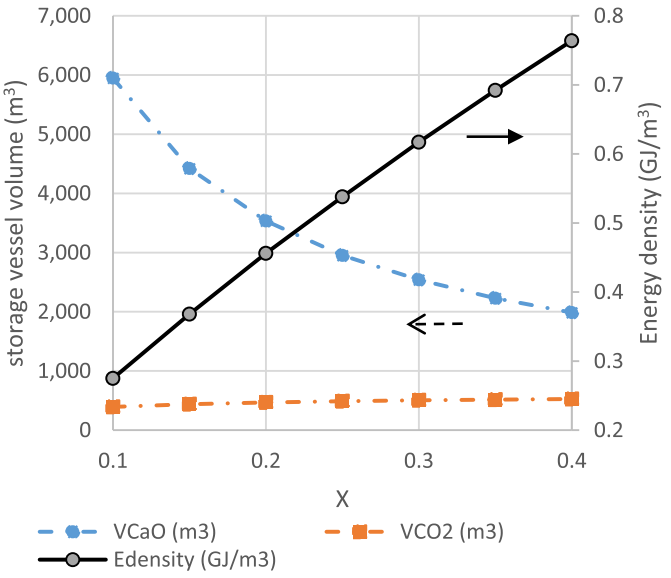

Fig. 10. Storage vessels and energy density as a function of CaO conversion. CO_2 is stored at 25 °C; 75 bar.

serves to enhance the overall net efficiency. These trends are also appreciated when overall average daily performance is considered.

As showed in section 2, the energy density of the storage system is highly influenced by the CaO conversion, as shown in Fig. 10. CO_2 vessel volume is not affected by X, but is only dependent on pressure and temperature conditions. Note that the energy density is calculated by using Equation (2), and therefore considers not only the CaCO3 as solid material, but also the CO_2 and CaO vessels, the bulk porosity and packing density of the granular solids. Thus, energy density of the storage system infrastructure varies between 0.27 and 0.77 GJ/m^3.

In Table 6 three more cases, in which temperature and pressure in the carbonator are varied taking into account thermodynamic equilibrium restrictions (Fig. 8), are analyzed.

As can be seen in Table 6, an increase of the carbonator temperature (and therefore of TIT) from 950 °C up to 1050 °C serves to enhance the overall plant efficiency by 0.8% points due to the increase of net power output in both the CO_2 and steam power cycles. As expected, an increase of the carbonator pressure (keeping fixed temperature) does not improve the cycle efficiency (as seen in Fig. 7 for other conditions). According to these results, the increase of the carbonator temperature improves the overall efficiency, albeit it would also add a higher degree of complexity for the tur-bine and the solid filtration system. On the other hand, varying the PR from 3 to 9 has an important effect on the heat exchanged in HXG (Table 6). This effect is caused by the reduction of the CO_2 temperature at the carbonator inlet, which decreases from 820 °C (at PR = 3) to 749 °C (at PR = 9) as a consequence of the isentropic CO_2 expansion process. A higher CO_2 temperature inlet allows a higher CO_2 mass flow rate to enter the power cycle since less car-bonator heat is used to preheat the reactants to the carbonator temperature. Thus, the CO_2 mass flow rate decreases from 395 kg/s (at PR = 3) to 231.3 kg/s (at PR = 9).

As a summary, case 3 simulation results indicate that increasing the temperature in the carbonator, and therefore the TIT, systematically leads to a higher overall plant efficiency. However, the maximum temperature in the carbonator is limited by the thermodynamic reaction equilibrium, which depends on the carbonator pressure. The process efficiency is also enhanced as the PR is increased up to a certain value of around 3–3.5 from which a further increase of the PR does not improve efficiency. Moreover, increasing the CaO conversion enhances the overall efficiency (reaching values about 43% at X = 0.4) mainly because of the significant reduction of auxiliaries power consumption for solids transport.

4.3. Effect of steam cycle conditions, auxiliaries consumption and turbomachinery-heat exchangers efficiencies

Following with the sensitivity analysis, this section assesses how the overall efficiency is affected by important parameters whose values were fixed in previous calculations (Table 1). Reference case conditions as well as the range of variation of these parameters are shown in Table 7. The values of those parameters not specified in Table 7 are left unchanged. Results of the sensitivity analysis on overall CSP-CaL efficiency are shown in Fig. 11.

Compared to CSP-CaL schemes reported in previous papers [8,21,37] a main novelty of the present work is the introduction of a steam power cycle to take advantage of the high temperature CO_2

Table 6
Energy balance for case 3 as a function of TIT and PR (without energy storage).

	Parameter	X = 0.15		
		$T_{carb} = 950\,^{\circ}C$ $P_{carb} = 3$ bar	$T_{carb} = 950\,^{\circ}C$ $P_{carb} = 9$ bar	$T_{carb} = 1050\,^{\circ}C$ $P_{carb} = 9$ bar
	Solar thermal power (MW_{th})	33.33	33.33	33.33
Heat exchangers (MWth)	HRSG	4.951	4.032	5.482
	GS-HE1	1.082	1.401	0.885
	COOLER-1	−0.128	−0.110	−0.128
	COND	−3.613	−2.941	−3.999
	COOLER-3	−5.283	−4.914	−4.232
	HXG	96.221	40.601	41.844
	GS-HE2	4.388	3.794	5.241
	GS-HE3	8.329	11.420	12.917
Power inlet (MWe)	Main CO_2 turbine (M-TURB)	25.702	27.245	25.974
	Steam Turbine (ST)	1.322	1.076	1.463
Power outlet (MWel)	Steam cycle pump (P)	−0.009	−0.008	−0.010
	Main CO_2 compressor (M-COMP)	−11.860	−13.503	−12.167
	Auxiliaries heat calciner	−0.030	−0.024	−0.033
	Auxiliaries heat carbonator	−0.105	−0.112	−0.100
	Auxiliaries solids transport calciner	−0.607	−0.546	−0.640
	Auxiliaries solids transport carbonator	−0.607	−0.546	−0.640
Carbonator heat (MWth)	carbonation heat	25.010	22.496	26.361
	reactants preheating (sensible heat)	−3.714	−3.893	−10.062
	losses	−0.250	−0.226	−0.258
	carbonator heat to power cycle	21.046	18.376	16.041
Power output CO_2 cycle (MWe)		13.842	13.741	13.807
Power output steam cycle (MWe)		1.313	1.069	1.453
Overall plant efficiency (η)		**0.414**	**0.407**	**0.415**

Table 7
Parameters variation throughout the sensitivity analysis on the overall CSP-CaL efficiency.

Selected scheme		case 3 (section 3.3)				
Main fixed parameters		TIT		950 °C		
		PR		3.5		
		X		0.15		
		SM		3		
Sensitivity analysis		Parameter	Ref. value	Variation		**ID-**Fig. 11
				lower limit	upper limit	
	Rankine cycle	live steam	400 °C;40 bar	360 °C; 40 bar	540 °C; 40 bar	**Rankine 1**
				360 °C;100 bar	540 °C; 100 bar	**Rankine 2**
	Turbomachinery isentropic efficiency	M-TURB	0.9	−5%	+5%	**Isentropic 1**
		HPS-TURB	0.8	−5%	+5%	**Isentropic 2**
		M-COMP	0.87	−5%	+5%	**Isentropic 3**
		HPS-COMP	0.8	−5%	+5%	**Isentropic 4**
	Turbomachinery mechanical efficiency	M-TURB	0.98	−2%	+2%	**Mechanical 1**
		HPS-TURB	0.96	−2%	+2%	**Mechanical 2**
		M-COMP	0.98	−2%	+2%	**Mechanical 3**
		HPS-COMP	0.96	−2%	+2%	**Mechanical 4**
	Turbomachinery intercooled stages	HPS-COMP	5	3	7	**HP-ic-stage**
		M-COMP	2	0	4	**LP-ic-stage**
	Heat exchangers minimum DT	HXG (regenerator)	15 °C	10 °C	20 °C	**HXG**
	Cooling temperature	Intercoolers	40 °C	30 °C	50 °C	**T-cooling**
		Cooler-2				
		Cooler-3				
	Heat exchangers pressure drops	Coolers	1%	−10%	+10%	**P-drops**
		HXG	5%			
		solid-gas HX	3%			
	Auxiliaries	Heat rejection	0.8% of heat released	0.4%	1.2%	**Heat-rejec**
		Solids conveying consumption	10 MJ/ton	5 MJ/ton	15 MJ/ton	**Solids**

stream exiting the calciner for power production. For this purpose, a simple Rankine cycle with moderate live steam conditions (400 °C/40 bar) has been considered from the small power output of this cycle (around 3 MW_e at plant design point). Considering these conditions, the net electric efficiency remains at 26.5% whereas for 540 °C/100 bar live steam conditions the efficiency increases by 5% points. By computing the overall efficiency after this live steam conditions change, the new efficiency value is 0.6%

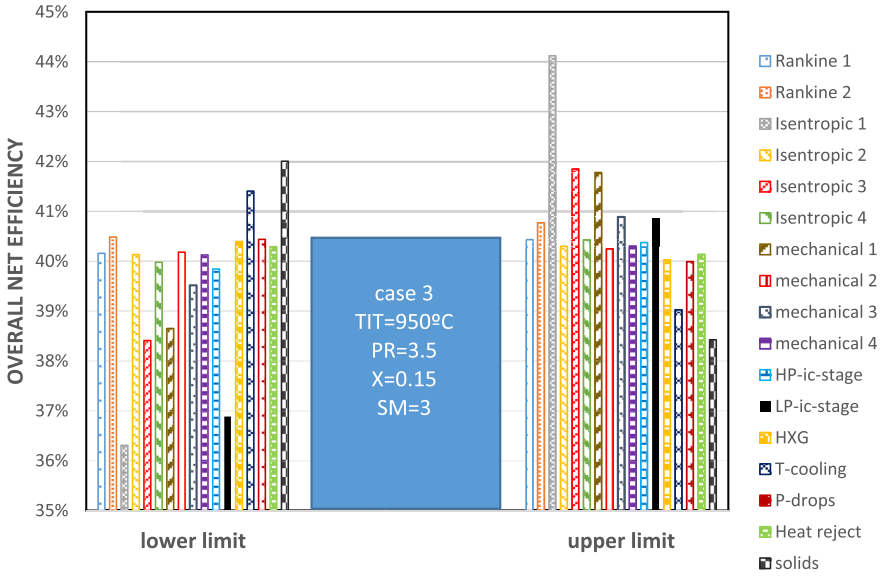

Fig. 11. Sensitivity analysis on overall CSP-CaL efficiency results (see ID definition in Table 7). For an easier understanding, bars are presented in the same order than legend and a colour code is used. The reader is referred to the web version of this article. (For interpretation of the references to colour in this figure legend, the reader is referred to the Web version of this article.)

higher than for the reference case.

As shown in Fig. 11, the most critical parameters on the overall efficiency are those related to turbomachinery efficiency. Thus, increasing by 5% the reference isentropic efficiency value for the main CO_2 compressor (M-COMP) the overall efficiency rises up to 44%. Regarding the number of intercooled stages, variations in low-pressure compressor have a stronger effect on the overall efficiency compared to the high-pressure compressor since the penalty over the cycle caused by the former is higher. Fig. 11 shows also that variations in energy consumption linked to solids transport plays a significant role in the plant efficiency, as was also seen in Fig. 9. Regarding heat exchangers, a reduction by 5 °C of the minimum temperature difference in the regenerator (HXG) leads to an enhancement of efficiency by 1%.

5. Conclusions

The present work is focused on an energy integration analysis of a CSP-CaL plant. Four novel integration schemes have been developed by progressively increasing the level of complexity. Plant operation considering solar multiples (SM) of 3 (design-point for a constant power production throughout the day) and SM = 1 (avoiding the energy storage equipment consumptions since lower solar radiation is assumed) were tested. As no high-pressure compressor is needed in the second case, the overall efficiency is increased by 1.8% points and therefore showing the penalty associated to the proposed high-pressure CO_2 storage system.

The base case presents an overall efficiency of 32.1%. By adding gas-solid heat exchangers on both the calciner and carbonator sides (case 2) the overall plant efficiency reaches a 34.7%. Furthermore, if a 2-intercooled stage compression is used in the low-pressure compressor (which is the equipment with greater energy consumption in the plant) efficiency is enhanced up to 38.1%. Cases 3 and 4 present similar efficiencies. The optimum configuration for a specific plant will depend on techno-economic considerations. Results from a sensitivity analysis on the pressure ratio (PR) in the Brayton cycle shows that the highest efficiency is achieved for PR around 3–4.5 in all cases.

A sensitivity analysis on the effect of CaO conversion and carbonator pressure/temperature shows that increasing the TIT under the limits posed by thermodynamic equilibrium enhances the overall plant efficiency. The overall efficiency is also enhanced as CaO conversion is increased (reaching values about 43% at X = 0.4), mainly because of the significant reduction of auxiliaries power consumption. A new expression for the energy density is proposed in this paper, which takes into account the size of the infrastructure (including all vessels and the packing density of solids). For the proposed cases, the energy storage density, mainly dependent on CO_2 pressure, CO_2 temperature and CaO conversion, varies between 0.2 and 0.9 GJ/m^3.

Our study gives support to the potential benefits of using the Calcium-Looping process for thermochemical energy storage in CSP plants. Major technological challenges are yet to be faced for the plant assessed in this work, especially related to the design of the solar receiver/calciner and to the high temperature solids pressurization and depressurization system. In future works, a design study of the solar receiver, hour-by-hour simulations of the plant considering variable heat input in the solar calciner and techno-economic analysis need to be undertaken to further assess the feasibility and competiveness of the CSP– CaL integration.

Acknowledgments

This work has been supported by the Spanish Government Agency Ministerio de Economia y Competitividad (MINECO-FEDER funds), contracts CTQ2014-52763-C2-2-R, CTQ2017-83602-C2-2-R and FPI contract granted to Carlos Ortiz Dominguez (BES-2015-0703149) within the project: Hybrid thermochemical storage of concentrated solar power (CTQ2014-52763-C2-2-R).

Appendix

Table 8 shows the main stream data for all simulated cases.

Table 8
Main stream data for the CSP-CaL integration

ID	Base case			Case 2			Case 3			Case 4		
	P (bar)	T (°C)	$\dot{m}$ (kg/s)	P (bar)	T (°C)	$\dot{m}$ (kg/s)	P (bar)	T (°C)	$\dot{m}$ (kg/s)	P (bar)	T (°C)	$\dot{m}$ (kg/s)
s1	1.10	850	72.19	1.20	850	53.47	1.20	850	53.06	1.00	850	53.27
s1-1	–	–	–	1.17	718.92	53.47	1.17	718.81	53.06	0.97	718.90	53.27
s1-2	–	–	–	1.14	665.03	53.47	1.14	659.62	53.06	0.94	662.40	53.27
s2	1.10	850	216.56	1.14	665.03	160.40	1.14	659.62	159.17	0.94	662.40	159.80
s3	–	–	–	1.11	692.17	160.40	1.11	687.39	159.17	0.91	689.84	159.80
c1	1.00	900	193.75	1.00	900	143.51	1.00	900	142.41	1.00	900	142.97
c2	1.00	900	64.58	1.00	900	47.84	1.00	900	47.47	1.00	900	47.66
v1	0.074	40.13	7.14	0.074	40.13	3.82	0.074	40.32	3.74	0.074	40.32	3.78
v2	45	40.53	7.14	45.00	40.53	3.82	45.00	40.72	3.74	45.00	40.72	3.78
v3	40	400	7.14	40.00	400	3.82	40.00	400	3.74	40.00	400	3.78
v4	0.075	40.32	7.14	0.075	40.32	3.82	0.075	40.32	3.74	0.075	40.32	3.78
g1	1.00	900	22.81	1.00	900	16.89	1.00	900	16.76	1.00	900	16.83
g1-1	–	–	–	0.97	692.17	16.89	0.97	687.39	16.76	0.97	689.84	16.83
g2	0.97	52.03	22.81	0.94	56.92	16.89	0.94	62.03	16.76	0.94	58.95	16.83
g3	0.96	40	22.81	0.93	40	16.89	0.93	40	16.76	0.93	40	16.83
g4	3.21	142.69	15.21	3.31	148.29	11.26	3.31	74.36	11.18	1.14	40	11.22
g5	75.75	123.66	15.21	75.75	124.27	11.26	75.75	124.27	11.18	75.75	124.27	11.22
g6	74.25	130	7.60	75.00	130	5.64	75.00	130	5.59	75.00	130	5.61
g7a	3.21	142.69	126.25	3.31	148.29	141.8	3.31	74.36	140.58	1.14	45.28	141.30
g7b	3.21	38.57	7.60	3.31	39.08	5.64	3.31	39.08	5.59	1.14	21.92	5.61
g8	3.21	138.83	133.72	3.31	143.44	142.38	3.31	72.78	141.19	1.14	72.81	142.14
g8-1	–	–	–	3.31	143.44	5.05	3.31	72.78	4.98	1.14	72.81	4.77
g8-2	–	–	–	3.21	665.03	5.05	3.21	659.52	4.98	1.10	662.39	4.77
g9	3.05	654.1	133.72	3.14	679.55	142.38	3.14	679.54	141.19	1.08	679.56	142.14
g9-1	–	–	–	3.14	679.05	147.43	3.14	678.87	146.17	1.08	679.00	146.91
g9-2	–	–	–	3.05	718.93	147.43	3.05	718.81	146.17	1.05	718.94	146.91
g10	3.00	850	126.25	3.00	850	141.8	3.00	850	140.58	1.00	850	141.30
g11	1.00	694.53	126.25	1.00	694.54	141.8	1.00	694.54	140.58	0.33	694.56	141.30
g12	0.95	153.83	126.25	0.95	158.65	141.8	0.95	87.98	140.58	0.32	88.01	141.30
g13	0.94	40	126.25	0.94	40	141.8	0.94	40	140.58	0.31	40	141.30

Notation

A	carbonator cross-section, m^2	$T_{i,\ vessel}$	storage temperature for of the i-component, °C
$c_{p,i}$	specific heat, kJ/(kmol·K)	TIT	turbine temperature inlet, °C
E_{den}	energy density, GJ/m^3	v_i	specific volume for the i-component, m3/kmol
ε_i	porosity of the i-component	V_i	storage vessel volume for the i-component, m^3
F_i	molar flow rate of component i, kmol/s	$\dot{V}_{CO2}$	CO_2 volume flow rate, m^3/s
F_{CaCO_3}	$CaCO_3$ molar flow rate	$\dot{W}_{net}$	average electrical power, MWe
$F_{CaCO3,crb}$	$CaCO_3$ molar flow rate (calciner side)	$\dot{W}_{net,night}$	net electrical power for the night mode, MWe
$F_{CaO,unr}$	molar flow rate of unreacted CaO (calciner side)	$\dot{W}_{net,sun}$	net electrical power for the sun mode, MWe
$F_{CO_2,clc}$	CO_2 molar flow rate at calciner outlet	$\dot{W}_{M-TURB}$	power produced by the main CO_2 turbine, MWe
$F_{CO_2,crb,in}$	CO_2 molar flow rate at carbonator inlet	$\dot{W}_{M-COMP}$	power consumed by the main CO_2 compressor, MWe
$F_{CO_2,crb,\ out}$	CO_2 molar flow rate at carbonator outlet	$\dot{W}_{HPS-TURB}$	power produced by the high-pressure CO_2 turbine, MWe
$F_{R,crb}$	recirculating molar flow rate (carbonator side)	$\dot{W}_{HPS-COMP}$	power consumption of high pressure intercooled CO_2 compressor for the storage system, MWe
$F_{R,clc}$	recirculating molar flow rate (calciner side)	$\dot{W}_{ST}$	power produced in the steam turbine cycle, MWe
h_i	Enthalpy, kJ/kmol	$\dot{W}_P$	power consumed in the steam turbine cycle, MWe
$\dot{m}$	mass flow rate, kg/s	$\dot{W}_{PSOLCAL}$	Power consumptions for solids transport in the calciner side, MWe
N	cycle number	$\dot{W}_{PSOLCAR}$	Power consumptions for solids transport in the carbonator side, MWe
P	pressure, bar	$\dot{W}_{AUXPOWCA}$	auxiliary power consumptions in the calciner side, MWe
P_{carb}	absolute carbonator pressure, bar	$\dot{W}_{AUXPOWCR}$	auxiliary power consumptions in the carbonator side, MWe
P_{eq}	CO_2 partial pressure at equilibrium, bar	X	average CaO conversion
PR	pressure ratio	X_r	residual CaO conversion
$\dot{Q}_{input}$	solar power input	ΔP	pressure drop at carbonator, bar
SM	solar multiple	Δt_{sun}	average daytime period (h)
T	temperature, °C	$\Delta H_R(T_{react})$	reaction enthalpy at the reactor temperature, kJ/mol
$T_{calciner}$	calciner temperature, °C	ΔH_R^0	standard enthalpy of reaction, kJ/mol
T_{carb}	carbonator temperature, °C	η	global net efficiency
T_{eq}	equilibrium temperature, °C	ϕ	packing density

References

[1] National Renewable energy laboratory (NREL). Concentrating solar power projects n.d. https://www.nrel.gov/csp/solarpaces/. [Accessed 2 April 2017].

[2] Li TX, Wu S, Yan T, Xu JX, Wang RZ. A novel solid−gas thermochemical multilevel sorption thermal battery for cascaded solar thermal energy storage. Appl Energy 2016;161:1−10. https://doi.org/10.1016/j.apenergy.2015.09.084.

[3] N'Tsoukpoe KE, Liu H, Le Pierrès N, Luo L. A review on long-term sorption solar energy storage. Renew Sustain Energy Rev 2009;13:2385−96. https://doi.org/10.1016/j.rser.2009.05.008.

[4] Kuravi S, Trahan J, Goswami DY, Rahman MM, Stefanakos EK. Thermal energy storage technologies and systems for concentrating solar power plants. Prog Energy Combust Sci 2013;39:285−319. https://doi.org/10.1016/j.pecs.2013.02.001.

[5] Pardo P, Deydier A, Anxionnaz-Minvielle Z, Rougé S, Cabassud M, Cognet P. A review on high temperature thermochemical heat energy storage. Renew Sustain Energy Rev 2014;32:591−610. https://doi.org/10.1016/j.rser.2013.12.014.

[6] Schmidt M, Linder M. Power generation based on the Ca(OH)2/CaO thermochemical storage system − experimental investigation of discharge operation modes in lab scale and corresponding conceptual process design. Appl Energy 2017;203:594−607. https://doi.org/10.1016/j.apenergy.2017.06.063.

[7] Singh A, Tescari S, Lantin G, Agrafiotis C, Roeb M, Sattler C. Solar thermochemical heat storage via the Co 3 O 4/CoO looping cycle: storage reactor modelling and experimental validation. Sol Energy 2017;144:453−65. https://doi.org/10.1016/j.solener.2017.01.052.

[8] Chacartegui R, Alovisio A, Ortiz C, Valverde JM, Verda V, Becerra JA. Thermochemical energy storage of concentrated solar power by integration of the calcium looping process and a CO2 power cycle. Appl Energy 2016;173:589−605. https://doi.org/10.1016/j.apenergy.2016.04.053.

[9] Bagherisereshki E, Tran J, Lei F, AuYeung N. Investigation into SrO/SrCO 3 for high temperature thermochemical energy storage. Sol Energy 2018;160:85−93. https://doi.org/10.1016/j.solener.2017.11.073.

[10] Rhodes NR, Barde A, Randhir K, Li L, Hahn DW, Mei R, et al. Solar thermochemical energy storage through carbonation cycles of SrCO3/SrO supported on SrZrO3. ChemSusChem 2015. https://doi.org/10.1002/cssc.201501023. n/a-n/a.

[11] Qu X, Li Y, Li P, Wan Q, Zhai F. The development of metal hydrides using as concentrating solar thermal storage materials. Front Mater Sci 2015;9:317−31. https://doi.org/10.1007/s11706-015-0311-y.

[12] Chen C, Aryafar H, Lovegrove KM, Lavine AS. Modeling of ammonia synthesis to produce supercritical steam for solar thermochemical energy storage. Sol Energy 2017;155:363−71. https://doi.org/10.1016/j.solener.2017.06.049.

[13] Sattler C, Roeb M, Agrafiotis C, Thomey D. Solar hydrogen production via sulphur based thermochemical water-splitting. Sol Energy 2017;156:30−47. https://doi.org/10.1016/j.solener.2017.05.060.

[14] Edwards JH, Do KT, Maitra AM, Schuck S, Fok W, Stein W. The use if solar-based CO2/CH4 reforming for reducing greenhouse gas emissions ruding the generation of electricity and process heat. Energy Convers Manag 1996;37(6−8):1339−44.

[15] Wentworth WE, Chen E. Simple thermal decomposition reactions for storage of solar thermal energy. Sol Energy 1976;18:205−14. https://doi.org/10.1016/0038-092X(76)90019-0.

[16] Barker R. The reactivity of calcium oxide towards carbon dioxide and its use for energy storage. J Appl Chem Biotechnol 2007;24:221−7. https://doi.org/10.1002/jctb.2720240405.

[17] Obermeier J, Sakellariou KG, Tsongidis NI, Baciu D, Charalambopoulou G, Steriotis T, et al. Material development and assessment of an energy storage concept based on the CaO-looping process. Sol Energy 2017;150:298−309. https://doi.org/10.1016/j.solener.2017.04.058.

[18] Benitez-Guerrero M, Sarrion B, Perejon A, Sanchez-Jimenez PE, Perez-Maqueda LA, Manuel Valverde J. Large-scale high-temperature solar energy storage using natural minerals. Sol Energy Mater Sol Cells 2017;168:14−21. https://doi.org/10.1016/j.solmat.2017.04.013.

[19] Kyaw K, Matsuda H, Hasatani M. Applicability of carbonation/decarbonation reactions to high-temperature thermal energy storage and temperature upgrading. J Chem Eng Jpn 1996;29:119−25. https://doi.org/10.1252/jcej.29.119.

[20] Sakellariou KG, Karagiannakis G, Criado YA, Konstandopoulos AG. Calcium oxide based materials for thermochemical heat storage in concentrated solar power plants. Sol Energy 2015;122:215−30. https://doi.org/10.1016/j.solener.2015.08.011.

[21] Ortiz C, Chacartegui R, Valverde JM, Alovisio A, Becerra JA. Power cycles integration in concentrated solar power plants with energy storage based on calcium looping. Energy Convers Manag 2017;149:815−29. https://doi.org/10.1016/j.enconman.2017.03.029.

[22] Meier A, Gremaud N, Steinfeld A. Economic evaluation of the industrial solar production of lime. Energy Convers Manag 2005;46:905−26. https://doi.org/10.1016/j.enconman.2004.06.005.

[23] Atsonios K, Grammelis P, Antiohos SK, Nikolopoulos N, Kakaras E. Integration of calcium looping technology in existing cement plant for CO2 capture: process modeling and technical considerations. Fuel 2015;153:210−23. https://doi.org/10.1016/j.fuel.2015.02.084.

[24] Dean CC, Blamey J, Florin NH, Al-Jeboori MJ, Fennell PS. The calcium looping cycle for CO2 capture from power generation, cement manufacture and hydrogen production. Chem Eng Res Des 2011;89:836−55. https://doi.org/10.1016/j.cherd.2010.10.013.

[25] Romeo LM, Lara Y, Lisbona P, Martínez A. Economical assessment of competitive enhanced limestones for CO2 capture cycles in power plants. Fuel Process Technol 2009;90:803−11. https://doi.org/10.1016/j.fuproc.2009.03.014.

[26] Martínez A, Lara Y, Lisbona P, Romeo LM. Energy penalty reduction in the calcium looping cycle. Int J Greenh Gas Control 2012;7:74−81. https://doi.org/10.1016/j.ijggc.2011.12.005.

[27] Cormos C-C. Economic evaluations of coal-based combustion and gasification power plants with post-combustion CO 2 capture using calcium looping cycle. Energy 2014;78:665−73. https://doi.org/10.1016/j.energy.2014.10.054.

[28] Barin I. Thermochemical data of pure substances. Weinheim: VCH; 1989. p. 1989.

[29] Flamant G, Hernandez D, Bonet C, Traverse J-P. Experimental aspects of the thermochemical conversion of solar energy; Decarbonation of CaCO3. Sol Energy 1980;24:385−95. https://doi.org/10.1016/0038-092X(80)90301-1.

[30] Fidaros DK. Baxevanou C a., Vlachos NS. A parametric study of a solar calcinator using computational fluid dynamics. Energy Convers Manag 2007;48:2784−91. https://doi.org/10.1016/j.enconman.2007.07.025.

[31] Meier A, Bonaldi E, Cella GM, Lipinski W, Wuillemin D. Solar chemical reactor technology for industrial production of lime. Sol Energy 2006;80:1355−62. https://doi.org/10.1016/j.solener.2005.05.017.

[32] Reich L. Towards solar thermochemical carbon dioxide capture via calcium oxide looping: a review. Aerosol Air Qual Res 2014;14:500−14. https://doi.org/10.4209/aaqr.2013.05.0169.

[33] Abanades S, André L. Design and demonstration of a high temperature solar-heated rotary tube reactor for continuous particles calcination. Appl Energy 2018;212:1310−20. https://doi.org/10.1016/j.apenergy.2018.01.019.

[34] Valverde JM, Barea-López M, Perejón A, Sánchez-Jiménez PE, Pérez-Maqueda LA. Effect of thermal pretreatment and nanosilica addition on limestone performance at calcium-looping conditions for thermochemical energy storage of concentrated solar power. Energy Fuels 2017;31:4226−36. https://doi.org/10.1021/acs.energyfuels.6b03364.

[35] Benitez-Guerrero M, Valverde JM, Perejon A, Sanchez-Jimenez PE, Perez-Maqueda LA. Low-cost Ca-based composites synthesized by biotemplate method for thermochemical energy storage of concentrated solar power. Appl Energy 2018;210:108−16. https://doi.org/10.1016/j.apenergy.2017.10.109.

[36] Edwards SEB, Materić V. Calcium looping in solar power generation plants. Sol Energy 2012;86:2494−503. https://doi.org/10.1016/j.solener.2012.05.019.

[37] Alovisio A, Chacartegui R, Ortiz C, Valverde JM, Verda V. Optimizing the CSP-calcium looping integration for thermochemical energy storage. Energy Convers Manag 2017;136:85−98. https://doi.org/10.1016/j.enconman.2016.12.093.

[38] Hanak DP, Manovic V. Calcium looping with inherent energy storage for decarbonisation of coal-fired power plant. Energy Environ Sci 2016;9:971−83. https://doi.org/10.1016/j.energy.2016.02.079.

[39] Le Moullec Y. Conceptual study of a high efficiency coal-fired power plant with CO2capture using a supercritical CO2Brayton cycle. Energy 2013;49:32−46. https://doi.org/10.1016/j.energy.2012.10.022.

[40] Binotti M, Astolfi M, Campanari S, Manzolini G, Silva P. Preliminary assessment of sCO2cycles for power generation in CSP solar tower plants. Appl Energy 2017;204:1007−17. https://doi.org/10.1016/j.apenergy.2017.05.121.

[41] Criado YA, Arias B, Abanades JC. Calcium looping CO2 capture system for back-up power plants. Energy Environ Sci 2017;10:1994−2004. https://doi.org/10.1039/C7EE01505D.

[42] Tregambi C, Montagnaro F, Salatino P, Solimene R. A model of integrated calcium looping for CO2 capture and concentrated solar power. Sol Energy 2015;120:208−20. https://doi.org/10.1016/j.solener.2015.07.017.

[43] Zhai R, Li C, Qi J, Yang Y. Thermodynamic analysis of CO2 capture by calcium looping process driven by coal and concentrated solar power. Energy Convers Manag 2016;117:251−63. https://doi.org/10.1016/j.enconman.2016.03.022.

[44] Hoffschmidt B. Receivers for solar tower systems. 2014.

[45] Ho CK. A review of high-temperature particle receivers for concentrating solar power. Appl Therm Eng 2016;109:958−69. https://doi.org/10.1016/j.applthermaleng.2016.04.103.

[46] Koepf E, Alxneit I, Wieckert C, Meier A. A review of high temperature solar driven reactor technology: 25years of experience in research and development at the Paul Scherrer Institute. Appl Energy 2017;188:620−51. https://doi.org/10.1016/j.apenergy.2016.11.088.

[47] SOLPART project. Temperature solar-heated reactors for industrial production of reactive particulates n.d. http://www.solpart-project.eu/(accessed June 1, 2017).

[48] Perejón A, Romeo LM, Lara Y, Lisbona P, Martínez A, Valverde JM. The Calcium-Looping technology for CO 2 capture: on the important roles of energy integration and sorbent behavior. Appl Energy 2016;162:787−807. https://doi.org/10.1016/j.apenergy.2015.10.121.

[49] Valverde JM, Sanchez-Jimenez PE, Perez-Maqueda L. Role of precalcination and regeneration conditions on postcombustion CO 2 capture in the Ca-looping technology. Appl Energy 2014;136:347−56. https://doi.org/10.1016/j.apenergy.2014.09.052.

[50] Valverde JM, Sanchez-Jimenez PE, Perez-Maqueda L. Ca-looping for post-combustion CO2 capture: a comparative analysis on the performances of dolomite and limestone. Appl Energy 2015;138:202−15. https://doi.org/

10.1016/j.apenergy.2014.10.087.
[51] Gil A, Medrano M, Martorell I, Lázaro A, Dolado P, Zalba B, et al. State of the art on high temperature thermal energy storage for power generation. Part 1—concepts, materials and modellization. Renew Sustain Energy Rev 2010;14:31–55. https://doi.org/10.1016/j.rser.2009.07.035.
[52] Abedin AH. A critical review of thermochemical energy storage systems. Open Renew Energy J 2011;4:42–6. https://doi.org/10.2174/1876387101004010042.
[53] Felderhoff M, Urbanczyk R, Peil S. Thermochemical heat storage for high temperature applications – a review. Green 2013;3:113–23. https://doi.org/10.1515/green-2013-0011.
[54] Guy E. Solar heat storage using chemical reactions. J Solid State Chem 1977;22:51–61.
[55] Prieto C, Cooper P, Fernandez AI, Cabeza LF. Review of technology: thermochemical energy storage for concentrated solar power plants. Renew Sustain Energy Rev 2016;60:909–29. https://doi.org/10.1017/CBO9781107415324.004.
[56] Valverde JM, Castellanos A. Random loose packing of cohesive granular materials. Europhys Lett 2007;75:985–91. https://doi.org/10.1209/epl/i2006-10208-4.
[57] Ortega-Fernández I, Calvet N, Gil A, Rodríguez-Aseguinolaza J, Faik A, D'Aguanno B. Thermophysical characterization of a by-product from the steel industry to be used as a sustainable and low-cost thermal energy storage material. Energy 2015;89:601–9. https://doi.org/10.1016/j.energy.2015.05.153.
[58] Kvamsdal HM, Romano MC, van der Ham L, Bonalumi D, van Os P, Goetheer E. Energetic evaluation of a power plant integrated with a piperazine-based CO 2 capture process. Int J Greenh Gas Control 2014;28:343–55. https://doi.org/10.1016/j.ijggc.2014.07.004.
[59] Mills D. Pneumatic conveying design guide. 2004. p. 80.
[60] Schorcht F, Kourti I, Scalet BM, Roudier S, Sancho LD. Best available techniques (BAT). Reference document for the production of cement. Lime and Magnesium Oxide 2015. https://doi.org/10.2788/12850.
[61] Kyaw K, Kubota M, Watanabe F, Matsuda H, Hasatani M. Study of carbonation of CaO for high temperature thermal energy storage. J Chem Eng Jpn 1998;31:281–4. https://doi.org/10.1252/jcej.31.281.